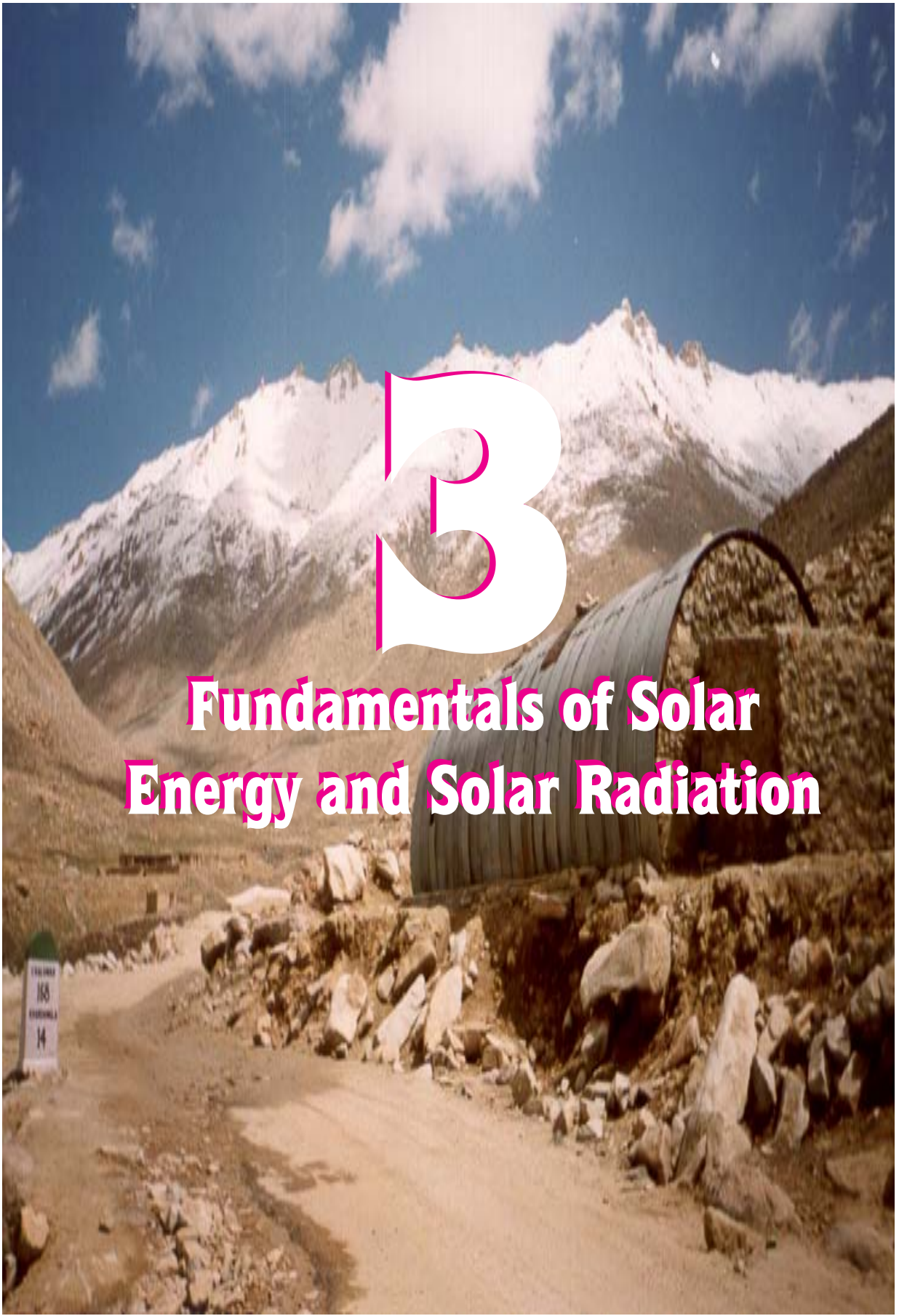

3

Fundamentals of Solar Energy and Solar Radiation

3.1
Fundamentals of Solar Energy

Ahmand Aga

Introduction

Earth receives radiant energy from the sun at the rate of 5.6 x 10^6 EJ/a (1 EJ = 10^{18} J). which is more than ten times the energy that is theoretically available from fossil fuels. The total energy available from fossil fuels that can be harnessed economically is only 0.5 per cent of the sun's energy (1.9 X 10^{14} tce). The world's currently available primary energy sources amount to about 9 x 10^9 tce, which is just 0.005 per cent of the annual solar radiation.

Solar radiation Quality

The emission spectrum of black body radiators is determined by their temperature. The spectrum of solar radiation outside the earth's atmosphere varies in relation to the emission of a black body at 6000° K; it is an almost continuous spectrum from about 200nm (nano-meter=10^{-9}m) of ultra-violet to 300nm of infra-red, with a strong peak around 500nm. Atmospheric absorption is to some extent selective, changing not only the quantity but also the spectral composition of the radiation received.

The shorter wave lengths represent a higher grade energy and all of the solar radiation can be considered for conversion to heat. But only the short wave, high energy component will be able to produce a photoelectric effect.

Quantity of Solar radiation

The intensity of radiation reaching the upper limits of our atmosphere, its mean value, 1395 W/m^2, is taken as the 'Solar Constant', and there is a variation of plus or minus

3.5 per cent due to the variation in the distance between the earth and the sun (152 x 10^4 km at the aphelion and 147 x 10^4 km at the perihelion).

Atmospheric absorption reduces this intensity to some extent, partly depending on the air mass through the atmosphere and partly on the state of the atmosphere (cloudiness. suspended particles). When the sun is at a low altitude angle, the intensity decreases. With a zenith position the intensity measured on a horizontal plane may approach one kW/m^2 (at sea level).

The annual total amount of radiation received at a given location depends on its geographical latitude and on local climatic factors. Solar radiation maps of the earth (as shown in Figure 3.1) give a rough indication of what can be expected at various locations.

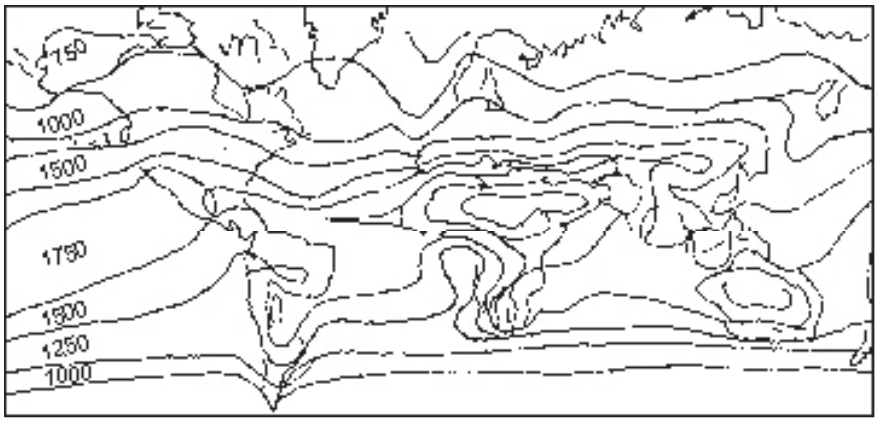

Figure 3.1: Solar Radiation Map of the Earth

Incident Radiation

If the radiation intensity on a tilted plane is to be calculated, the total radiation as measured on a horizontal plane must be divided into direct and diffuse components. The direct component will then be handled vectorially. The diffuse radiation incident on the tilted plane will be proportionate to the fraction of the sky's hemisphere to which the plane is exposed.

The relationship between the sun and any building can be examined from two points of view.

1. Exclusion of solar radiation as it would cause overheating. An extra load on air conditioning. glare problems, or deterioration of materials.
2. Ensuring adequate sunlight to obtain heat when it is in short supply or purely for its psychological effect.

There is no doubt that, in tropical climates, the first point will dominate, whereas in cold winter regions the latter will prevail. It has been shown, however, that, even in moderate

climates, severe overheating can occur. All glass walls have been proved to be thermally inferior to solid walls with small windows, as glass walls result in large heat gains in summer. The use of extensive glazing on south-facing walls has been advocated. Such buildings are described as solar housing. The apparent contradiction can be resolved in terms of time. Both statements may be true at different times of the year. For example, for a particular solar house, 33 per cent of the heat required is gained through the windows, 49 per cent by the collector system, and 18 per cent by an auxiliary heat source. Another type of building can be designed to be heated exclusively by solar heat gain through the windows. Solar heat gain through the windows is common even in winter, and its magnitude can be verified by means of the following simple calculation.

If indoor temperature, t_i = 20°C
Outdoor temperature, t_o = 0°C
Thermal transmittance is taken as, U = 5 W/m^2°C
Radiation Intensity I, = 400 W.m^2
Solar gain factor, g = 0.8
For 1 m^2, we have Q loss = 5 x 20 = 10 W/m^2, Q gain = 400 x 0.8 = 320 W/m^2

The gain is more than three times the loss. However, the above is true only for the period of sunshine. Even if we take a sunny day in winter, for the 24-hour period the total loss may be greater than the total gain.

At the very best, in December and January. a south-facing wall may get over 200 W.h/m^2 of radiation a day. The heat loss during the same 24 hours may be 2400W.h/m^2 and most days will have much less radiation than cited. Double glazing would improve the situation, but, clearly, what is needed is some form of control of solar gain and coordinated control of all the thermal factors of the building.

The position of the sun at any point in time is defined in terms of two angles: altitude (a) and azimuth (g) (Figure 3.2 shows the Solar Geometry).

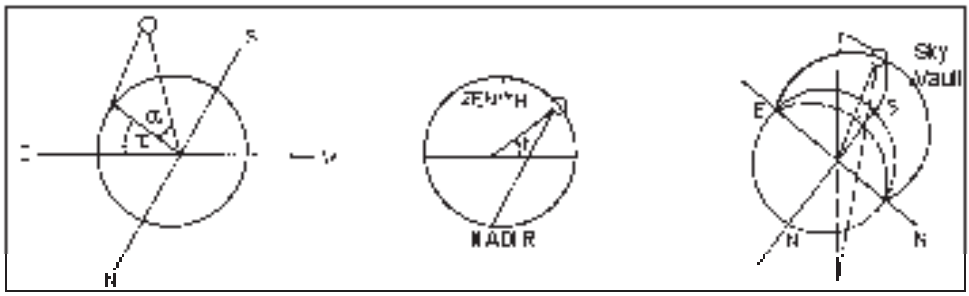

Figure 3.2: Solar Geometry

These angles can be found for any hour of the year from almanacs or from sun-path diagrams of various kinds. By far the best known of these are the stenographic solar charts (Figure 3.3). The two angles can be read directly (as shown in Figure 3.3):

γ. or the azimuth angle by projecting the time point from the Centre to the Perimeter scale.
α. or the altitude angle

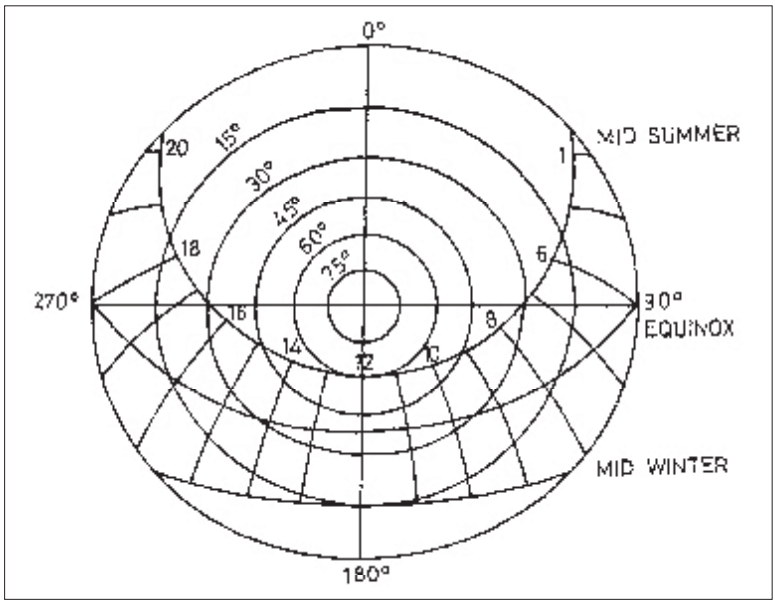

Figure 3.3: Solar Charts Giving Altitude and Azimuth Analysis

If the sun's position is to be related to the building or rather to a particular vertical wall of the building, shadow angle protractors (Figure 3.4) have to be used. This will give readings of two additional angles (Figure 3.5):

d, or the horizontal shadow angle, the azimuth difference (if any orientation, i.e., the wall a azimuth is w, then d = w -γ) and

e, or the vertical shadow angle, i.e., the altitude angle of the sun, projected parallel to the wall on to a vertical plane which is perpendicular or the wall. This will normally be the plane of assertion of the building when d is zero, i.e., the sun is directly opposite the wall, e = in all other cases e-a, the relationship can be expressed as

tan e=sec d/tan α.

On the basis of plans and sections, the shading mask of any device can be constructed by using the protractor when this shading mask is laid immediately along the date and hour lines.

The size and physical make-up of devices do not matter from the point of view of geometry; many different devices can give the same performance. Thus, early on in the process, the designer may decide what the required shading performance is, i.e., the shading mask, still preserving his freedom to select the actual device.

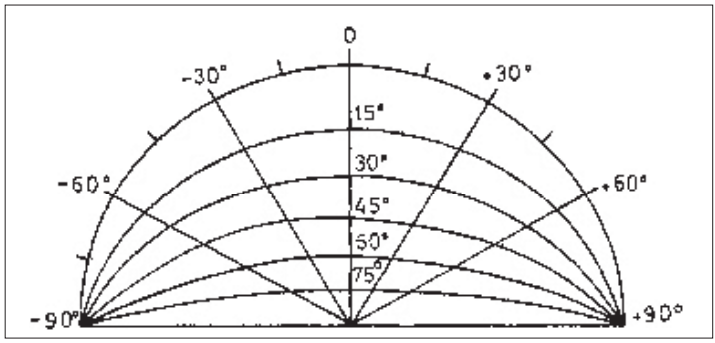

Figure 3.4: The Shadow Angle Protractor

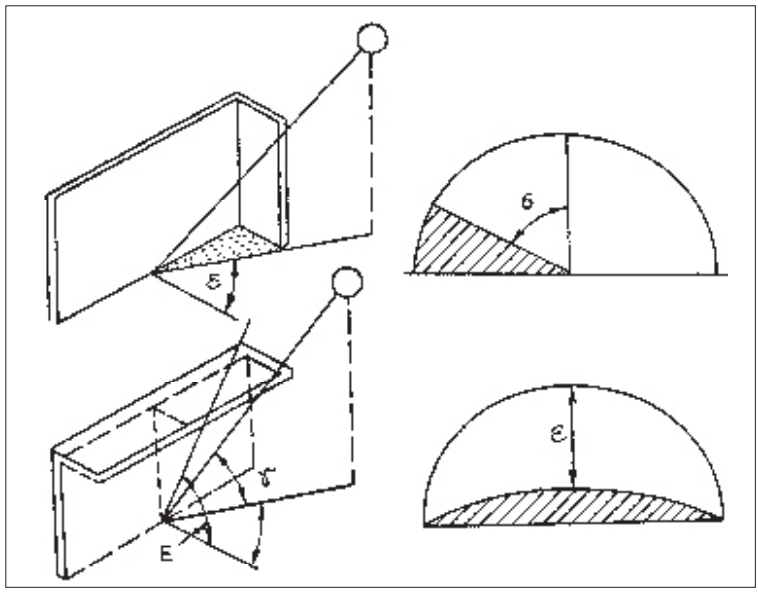

Figure 3.5: Shadow Angles

Fixed shading devices are purely negative controls, i.e., they exclude the sunshine. Adjustable shading devices (louvers) can be used, but they are rather expensive. However, even fixed devices can be designed to give selective performance, i.e., to admit the sun when it is desirable and exclude it when it would cause overheating. The period of overheating can be outlined on the sun path diagram and a shading mask constructed to match the shape of the overheated period as closely as practicable.

Shades over a south-facing window would exclude the high altitude summer sun but admit the radiation in winter when the sun is at a low angle. It is also shown how this is reflected by the shading mask and sun-path diagram. There is a close match between the shape of the overheated period and the shading mask.

Special glass can also be used for solar control. Heat-absorbing glass has selective absorption properties, whilst heat-rejecting glass has selective reflectance (Figure 3.6)

A. Glass with Fe_20_3 content, 6 mm
B. Polymethyl methacrylate sheet, 6 mm
C. PVC film 0.035 mm

Figure 3.6 gives the spectral transmission characteristics of certain types of glass and diagra mmatic representation of the reflection/transmission/absorption/re-emission processes. These special types of glass will reduce the radiant heat transmission, but, once installed, they will act as controls all the time, and there is no differentiation between summer and winter conditions.

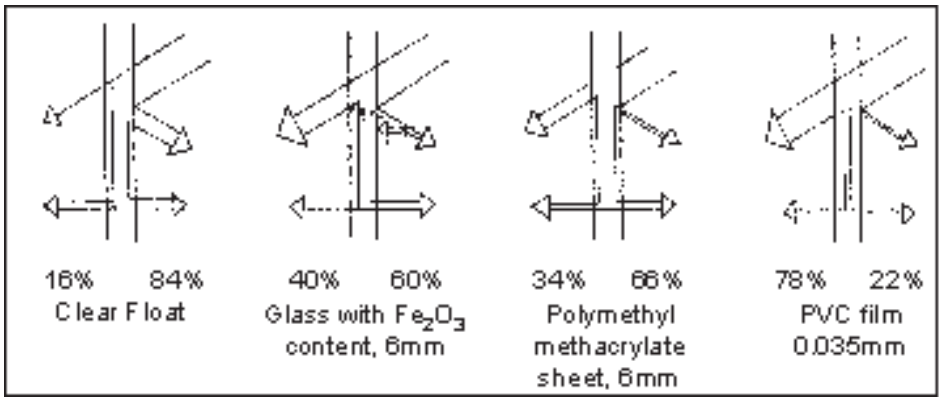

Figure 3.6: Spectral Transmission Characteristics of Selected Types of Glass

The concept of the building as a 'Climate Filter' is a reality and further it should be a selective filter, admitting environmental influences that are desirable and excluding the undesirable ones. Solar controls, both shading device and special types of glass, may be considered as selective filters. Their performance, however, cannot be considered in isolation. They will thermally interact with the whole building and its functions. The thermal behaviour of the building will be determined by factors such as:

1. window size and orientation,
2. type of glazing and any shading device,
3. surface qualities, size, and exposure of solid elements; and also by

1. thermal insulation of enclosing elements,
2. thermal capacity of the building fabric,
3. the relative position of insulation and its capacity, and
4. ventilation and its variability.

All these factors must be considered in relation to the use of the building and heat output of the lighting and of persons and processes in the building and the periodicity

of these. The designer must be a conductor, coordinating the orchestration—the performance of a multitude of instruments.

In some situations. the means listed above, i.e., the passive thermal controls, may achieve satisfactory indoor conditions. Yet, even if comfort cannot be ensured by such means alone, a good design will reduce the task of active controls greatly, i.e., of installations using some form of energy input such as heating and air-conditioning.

3.2 Climatology and Passive Solar Building

H.B. Karki

Introduction

The climate of a particular place is closely related to the daily and monthly variation in solar radiation over the entire year. For passive solar building design, an understanding of solar energy in terms of sunbath, location, and intercepted solar energy is essential. The factors that affect the availability of solar energy are (1) geographic location; (2) site of the building; (3) orientation; (4) time of the day; (5) season of the year; (6) atmospheric conditions. i.e., clouds, water vapour, dust particles, and pollutants; and (7) building design. Some of these aspects are discussed below.

Basic Solar Geometry

There are two major motions of the earth: the revolution of the earth around the sun and the spinning of the earth on its own axis. Both motions play an important role in solar energy applications.

The earth's positions, tilted in relation to its orbital plane around the sun, provide the geometric basis for the annual variation of solar energy received on the earth's surface (Figure 3.7). The earth's polar axis is tilted 23° 27' (~ 23.5°) in relation to the plane of the earth's orbit around the sun. This plane is geometrically described by the sun-earth line, also called the solar elliptic plane. It is useful to visualise the sun- earth line as a cluster of parallel light beams. On two days in the year, March 21 and September 21 (The Spring and Autumn equinox), the sun's beams are parallel to the earth's equatorial plane. From the earth's point of view, on these two dates the sun rises and sets in the east and west, respectively. From the sun's position, an observer would see the east tilt at 23.5 in relation to the elliptic plane.

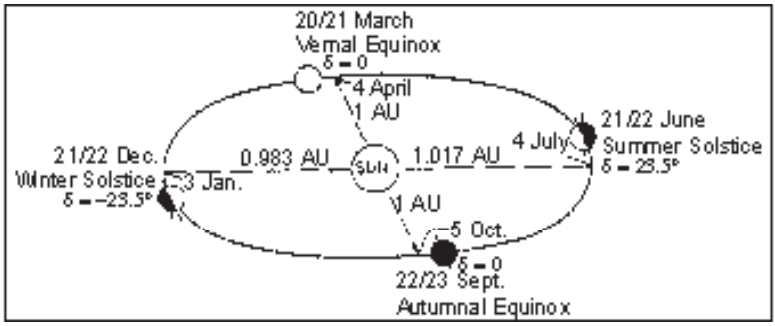

Figure 3.7: Motion of the Earth around the Sun

The angle measured by any point on the earth's surface between the sun-earth line and the plane defined by the earth's equator is the solar declination (Kreider and Kreith 1981), which is given as

$$\delta = 0.398 \cos [0.986 (N-10)] \quad (3.1)$$

where, N is the number of days counted from January 1st.

The earth revolves in an elliptical orbit with the sun at one focus of the ellipse. The magnitudes of the semi-major axes and semi-minor axes are 1.4968×10^8km and 1.4966×10^8km respectively. The period of the earth's revolution about the sun defines one year. The perihelion (the position of the earth nearest to the sun) occurs on approximately the second of January and the aphelion (the position at the maximum distance) occurs on July 2. The declination provides a measure of the variation of positions on a seasonal basis.

To understand sun angles for the purpose of building design, the earth's orbit can be considered circular with the sun at its centre. In fact, the orbit is an ellipse; with the sun being off-centre. Orbital speed slows down as the earth moves closer to the sun and accelerates as it moves away. The eccentricity and obliquity of the earth's orbit result in a difference between solar time, measured by the sun's position in the sky, and standard time, measured by ordinary clocks running at constant speed. The equation used to correct discrepancies between solar time and standard time is given as:

$$t_{sol} = ts + E + 4 (\beta - \phi) \quad (3.2)$$

where, E represents the equation of time

$$E = 12 + (0.1236 \sin x - 0.0043\cos x + 0.1538\sin 2x + 0.0608\cos 2x)$$

and where t_s is local standard time and the angle is x

$$x = \frac{360(N-1}{365.242} \quad (3.3)$$

To an observer on earth, the sun appears to revolve around the earth once a day. If this path could be observed for 24 hours, the sun's rays (the sun-earth line) would describe a solar ray cone drawn between the sun and earth. The shape of the cone varies each day according to the sun's declination (Figure 3.7). Coincidence with the ecliptic, the solar ray cone would in fact be a flat plane on the equinox dates.

The sun's path can be traced in various ways, by making a dome overhead with the observer on earth at the centre, the sun's apparent path would be traced on the dome as it intersects the solar ray cones or by a vertical cylindrical graph as shown in Figure 3.8.

The sun's position on the celestial sphere is usually given in terms of solar azimuth angle, α, and the solar altitude, a. These are shown in Figure 3.9. The altitude angle measures the sun's angular distance from the horizon and the azimuth angle, α, measures the angular distance from the south. The solar zenith angle, z, is the sun's distance from the zenith, which is the point directly overhead on the celestial sphere. Thus, a and z are complementary angles.

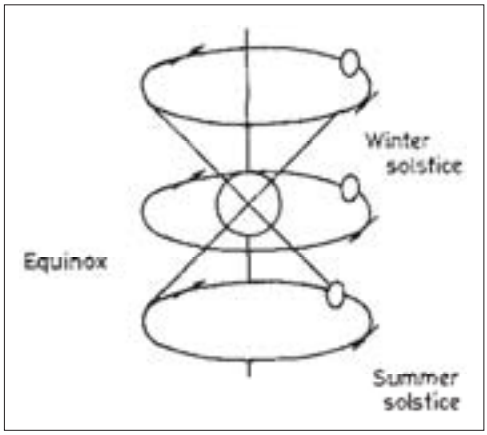

Figure 3.8

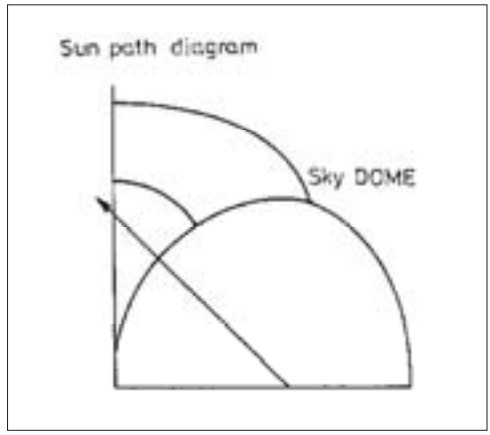

Figure 3.9

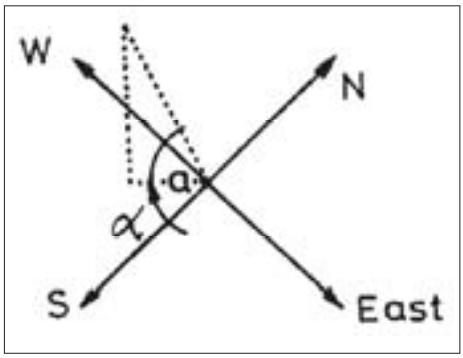

Figure 3.10

$$a + z = 90^\circ \quad (3.4)$$

The solar altitude and azimuth angles are computed for any time date and location by using the following formula (Dickson and Cheremisinoff 1980):

$$a = \sin \phi \sin \delta + \cos \phi \cos \delta \cos h_s \quad (3.5)$$

where f is the latitude taken at positive north of the equator.

$$\sin\alpha = \frac{\cos\delta \sinh_s}{\cos\beta} \qquad (3.6)$$

and h_s is the solar hour angle and equal to 15 (12- t_s).

Sunset and sunrise occur when the solar altitude angle is zero. Then from equation (3.5) we have

$$\cos h_{sr} = \tan\delta \times \tan\phi \qquad (3.7)$$

where,

h_{sr} (sunrise) = - h_{ss} (sunset)

The intensity of solar radiation on a surface depends upon the angle at which the sun's

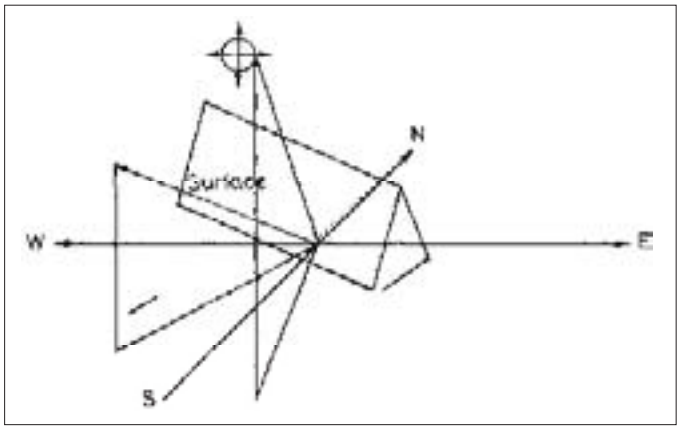

Figure 3.11

rays strike the surface. For a fixed surface:

$$\cos i = \cos\delta \cos(\phi-\tau) \cos h_s + \sin\delta \sin\tau \qquad (3.8)$$

where, τ is the angle of tilt.

At a particular hour of the day or day of the year, the environment casts a shadow on the surface. To calculate quantitative shading, the shading profile angle is required and from Fig 3.12 we have

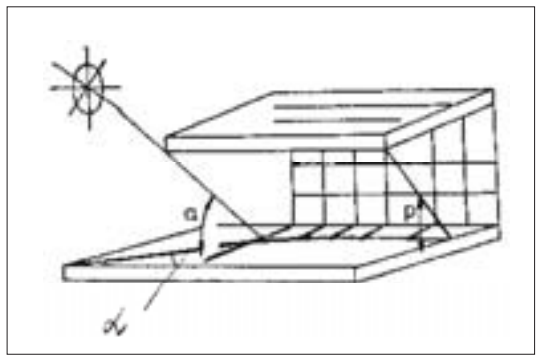

Figure 3.12

$$\tan p = \frac{\tan a}{\tan \alpha} \qquad (3.9)$$

$$d = \frac{\sin \tau + p}{\sin p}$$

Radiant Energy

Radiant energy is usually described as a stream of particles called photons, travelling in a transverse wave at the speed of light, c. Each photon possesses a wavelength and an amount of energy, E. These are related by the equation

$$E = \frac{hc}{\lambda} \qquad (3.11)$$

where h is Plank's constant, h = 6.6 x 10^{-34} Js. and c = 3 x 10^{8} m/s, the velocity of light, it may be expressed as:

$$E = h\nu \qquad (3.12)$$

since, $\nu = \frac{c}{\lambda}$

Solar radiation covers a fairly wide range of wave lengths. The approximate distribution of solar radiation in relation to wavelength has been shown in Figure 3.13.

Solar radiation is considerably altered in its passage through the earth's atmosphere. The two important mechanisms causing these atmospheric changes are absorption and scattering. There are several atmospheric constituents that absorb part of the incoming radiation. The first one is ozone, and it absorbs all the ultraviolet solar radiation.

The other absorbers are water vapour, carbon dioxide, oxygen, and other gases and particles. The water vapour absorbs specific wavelength bands in the infrared region. consequently the spectral distribution of radiation contains several pronounced dips and peaks in the infrared region.

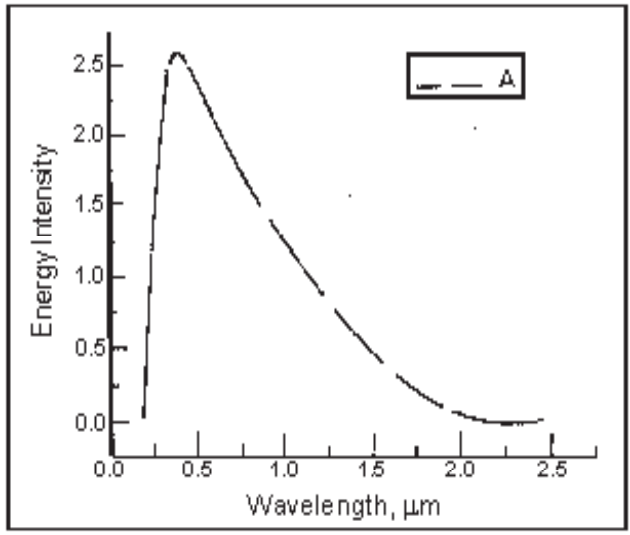

Figure 3.13: Distribution of Solar Radiation

The amount of water vapour in the atmosphere depends upon the local altitude, climate, and season. Since warm air can hold more water vapour without precipitation than cold air, the variation in atmospheric water vapour is generally higher in summer than in winter. The effect of this is a variation in solar intensity of from 5 to 20 per cent. In addition to this, scattering also produces considerable effects. Clouds' scattering reduces the incoming radiation intensity by 80 to 90 per cent through single multiple scattering, because it returns the incoming radiation to space. The solar radiation that travels through the atmospheric path, defined in terms of air mass (m), is calculated as:

$$m = \sec z. \tag{3.13}$$

However. for the spherical earth, eq 3.13 is valid only for zenith angles of less than 70°. The adjustment in air mass for local altitude is made in terms of the local atmospheric pressure (P). The adjustment is:

$$m = m_o \frac{P}{P_o} \tag{3.14}$$

where, P is the mean pressure and m_o and P_o are corresponding air mass and pressure at sea level.

In addition to this. spectral mass also has a considerable effect.

There are various types of instrument to measure solar radiation, both direct and diffused radiation. Among them are a) normal incidence pyrheliometers and b) pyranometers.

3.2.3 Figures of Merit of Passive Systems

From the first principle of thermodynamics, efficiency is the ratio of net useful heat energy to the total solar energy incident on the collecting surface. The corresponding efficiency for natural cooling is the ratio of net energy removed from the building to the total energy lost from the radiative cooling element of the building. Over an extended time period, the efficiency of a natural cooling system must be unity. This is also commonly known as figures of Merit of passive systems (Kreider and Kreith 1982)

Solar heating contribution: This is perhaps the most useful and least ambiguous figure of merit. it is simply the net energy contributed to the building by the passive solar element. The figure of merit is needed to compute the cost effectiveness of the system.

Solar heating fraction: The solar heating fraction (f) is the ratio of net energy provided to the building by the passive solar elements to the total heat required (Kreider and Kreith 1982; Yannas [ed.] 1983). Thus

$$f = 1 - \frac{Q_a}{L} \tag{3.15}$$

where Q_a is the auxiliary heating required. L is the total load of the building.

Historical Perspective : Passive Building Systems

The majority of passive systems for space heating can be placed within one of five generic system types (Kreider and Kreith 1982; Yannas [ed.] 1983; Mazaria 1987).

Types of passive system
1. Direct Gain
2. Thermal Storage-Wall
   - •Masonry Walls
   - •Water Walls
3. Solar Green House
4. Convection Loop
5. Thermal Storage Roof

Basic design elements are:
- thermal insulation of the buildings,
- solar energy collection,
- thermal storage,
- solar gains,
- sun angle considerations, and
- solar penetration through glass.

A direct gain system admits sunlight into the space to be heated. The system aperture is usually double pane glass, always located on the south faces of buildings (Figure 3.13). The interior material of the building is capable of absorbing sufficient energy through radiation and convection, shutters, reflectors, and roof overhangs are methods for increasing or decreasing gain at varying times of the day and year.

Convective Loops

Convective loops use an absorber surface to absorb incident radiation and then convect warm air into the building space (Figure 3.14).

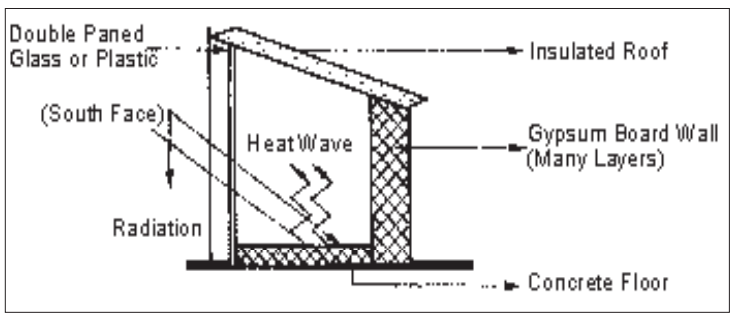

Figure 3.14

There are three types of storage system, short-term storage-lasting for a few hours only; diurnal heat storage-consisting of heat stored during the day that is returned at night; and long-term storage which refers to storage lasting longer than one day. Of these. diurnal storage is the most significant for passive solar designs.

Diurnal storage is the capacity to store heat according to each degree of temperature swing ($Q_d = \Delta Q/\Delta T$). Heat capacities for various types of material are given in Table 3.1.

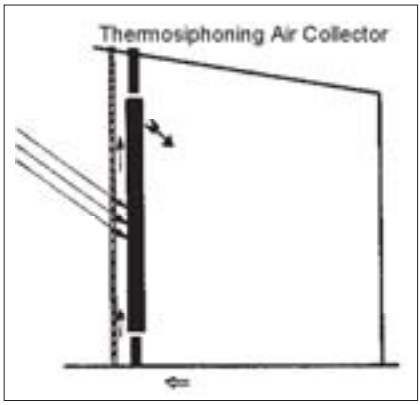

Figure 3.15

The diurnal heat capacity of a whole room is given as:

Table 3.1: Heat Capacities of Different Materials

Material	Density kg/m^2	Specific Heat Kcal/°C kg	Thermal Conductivity W/m °C
Granite	2675	0.20	1.8
Concrete	2290	0.21	1.72
Concrete Masonry	2242	0.12	1.42
Limestone	2452	0.22	0.92
Builder's Bricks	1922	0.22	0.72
Adobe	1922	0.20	0.56
Hardwood	720	0.2	0.16
Softwood	512	0.22	0.12

$$Q_D = \Sigma_i A_i Q_i \qquad (3.16)$$

where A_i is the area of the first surface, and

Q_i is the diurnal heat capacity of i^{th} surface.

The main use of diurnal heat capacity is for estimating room temperature swing. From this, heat balance is calculated over a 12-hour period in the day, accounting for solar gain plus internal heat losses. The heat losses are calculated based on the heat loss coefficient of the building and the difference between the average inside temperature and the outside ambient temperature. The energy balance yields the following mathematical expression:

$$\Delta T = \frac{Q_s A - (T_r - T_a)H/2 = Q_i/2}{Q_D} \qquad (3.17)$$

where,
ΔT = room temperature swing
T_r = daily average room temperature
T_a = daily average ambient temperature
Q_s = daily solar gain per unit area of direct gain glazing
Q_i = daily internal heat
H = heat loss coefficient of the building
A = direct gain glazing area.

If one wishes, one can account for the detailed structure of the inside and outside hourly temperature profile to determine Q_s and T_r.

Convection through doorways can be estimated from the following relationship:

$$Q_c = 63.5\, W_d\, (H_d\, \Delta T)^{3/2} \qquad (3.18)$$

where,
Q_c = heat flow
W_d = doorway width
H_d = doorway height
ΔT = room to room temperature difference

The main disadvantages of passive designs is that they usually require integration of the solar collection and storage function into the architecture of the building. Thus the solar energy system is an integral part of the building. This integration of function is not the contemporary approach to architectural design. If passive techniques are integrated

BIBLIOGRAPHY

Dickson, W.C.; Cheremisinoff, P.N., 1980. *Solar Energy Technology Handbook*, Part B. Place not given: Marcel Dekker.

Kreider J.F. and Kreith F., 1981. *Solar Energy Handbook*. New Delhi: McGraw-Hill.

Kreider. J.F. and Kreith F., 1982. *Solar Heating and Cooling*. New Delhi: McGraw - Hill.

Krith F. and West R.E., 1980. Economics of Solar Energy and Conservation Systems, Vols 1 and 2. Place not given: CRC Press.

Mazaria E., 1987. *The Passive Solar Energy Book*. Place not given: Rodale Press 1979.

McVeigh, J.E., 1977. *Sun Power.* New York, USA: Pergamon Press.

Yannas S., 1983 (ed). *Passive and Low Energy Architecture*. New York, USA: Pergamon Press.

3.3
The Spectral Characteristics of Global Radiation and Surface Albedo on the Northern Tibetan Plateau

Zou Jiling and Ji Guoliang

Introduction

In order to understand the spectral characteristics of total solar radiation and global surface albedo on the Qinghai and Tibetan Plateau while studying absorbed energy and output energy affected by global surface nature, total solar radiation and global surface albedo were observed in Wudaoliang. This is useful information for developing plant photosynthesis in the region.

Wudaoliang (35° 17' N & 93° 06' E) is located in the northern part of Qinghai and the Tibetan Plateau, between Kulun and Tanggual mountains. Its altitude is 4,612 m, and it has a sub-freezing, partially dry climate and the vegetation type is that of a sparse plain (Zhenyao and Xiangding 1981). The observation area is quite wide. The soil is sandy and supports sparse grass in summer. This paper reports on information collected for the period between August 1993 and July 1994 during 25 sunny days.

The paper analyses radiation flux of four bands, upward and downward: the total solar radiation band (0.3 to 2.8 mm), the ultraviolet radiation band (0.3-0.4 μm), the blue-purple radiation band (0.4-0.5- mm), and the near infrared radiation band (0.7-2.8 mm). A total spectral radiation apparatus (TBQ-4-1 model) produced in China was used in order to observe all bands. Two pieces of equipment were used to observe upward and downward components. The apparatus parameters are given in the references (Hao 1993). The apparatus was used to observe solar radiation along the Heihe River, and it demonstrated that the calibration is stable and the information reliable.

Total Spectral Radiation

Daily Variation in Spectral Radiation

The daily average variation in radiation showed that visible light energy is high at noon and low in the early morning and late afternoon; near-infrared radiation energy is high in the early morning and late afternoon and low at noon. The reason for this is that solar altitude is low in the early morning and late afternoon. Atmospheric thickness is broad and short waves are easily affected and weakened by all kinds of gases in the atmosphere, so that the long wave fraction is comparatively big. When solar altitude is higher, the atmospheric thickness is smaller, and short waves are less weak, infrared radiation energy is attenuated, and thereafter the visible light energy increases. The results are in agreement with the results observed in the Hexi region.

Seasonal Variation of Spectral Radiation

Table 3.2 gives the ratio of spectral band energy to total band radiation energy during four seasons of the year. The table shows that: (a) the energy of each band has different variations in different seasons. Ultraviolet is low in winter and high in summer, which is different from the seasonal variations in the plains; blue-purple radiation and near-infrared radiation are high in winter and low in summer. This is because the wind velocity is intense near the global surface, and there is a lot of dust in the atmosphere in winter and spring; the aerosol content increases in the air, so that short-wave energy is weakened; and visible-light is intense and infrared radiation low in summer. The table also shows that (b) the year's average radiation energy of ultraviolet is 4.8 per cent of the total radiation. The blue-purple content is 14.8 per cent; visible-light is 50.3 per cent, and near-infrared light is 49.8 per cent. The ultraviolet and blue-purple radiation intensities in Wudaoliang are higher than in the plains. The infrared radiation in Wudaoliang is lower than in the plains. The results are in accordance with earlier studies. The greater the blue-purple radiation ratio the better it is for formation of plant proteins and fat.

Table 3.2: Spectral Energy Ratio Distribution to Total Radiation (%)

Season	0.3-0.4 μm	0.4-0.5 μm	0.3-0.7μm	λ <0.7 μm	0.4-0.7 μm
Spring	4.7	14.5	50.0	50.0	45.3
Summer	5.1	12.0	51.8	48.2	46.7
Autumn	4.9	15.4	50.5	50.0	45.6
Winter	4.4	16.2	49.0	51.0	44.6
Average	4.8	14.8	50.3	49.8	45.5

Radiation energy for $\lambda \geq 0.7$ mm and $l < 0.7$ mm was calculated. Table 3.3 gives the average solar radiation for $\lambda \leq 0.7$ mm. In Wudaoliang, the intensity for $\lambda < 0.7$ mm in summer is more than in other parts of the country (Hexi Luzhoce) and than in Europe. This is because of the clear atmosphere due to high altitude.

Table 3.3 shows efficient radiation associated with plant photosynthesis (0.4-0.7 mm). It has the following characteristics: (a) the efficient radiation energy associated with

photosynthesis is greater in Wudaoliang compared to Hexi Luzhou and (b) the efficient radiation changes with season, its energy ratio is higher in summer and lower in winter, and this conforms to results observed in the Hexi region.

Table 3.3: Comparison of the Energy Ratio of Two Bands to Total Radiation

Season	Spring		Summer		Winter	
	$\lambda > 0.7$ μm	$\lambda < 0.7$ μm	$\lambda > 0.7$ μm	$\lambda < 0.7$ μm	$\lambda > 0.7$ μm	$\lambda < 0.7$ μm
Hexi Luzhou	56	44	53	47	56	44
China	52	48	50	50		
European	51	49	48	52		
Wudaoliang	50	50	48	52	51	49

Solar Spectral Albedo

Using total spectral solar radiation and global albedo radiation. the solar spectral albedo in Wudaoliang was determined. Daily variation and seasonal variation in spectral albedo are discussed below.

Daily Variation in Spectral Albedo

Daily variation in visible-light albedo and near infrared radiation albedo for $\lambda > 0.7$ mm and $\lambda < 0.7$ mm is calculated, respectively. It was found that:

(a) A_v (visible-light albedo), A_N (global surface albedo), and A_k (total band albedo) are similar in daily variation, high in the early morning and late afternoon and low from 9.00 - 15.00 (this is due to the low sun angle in the early morning and late afternoon, which is weakened by the atmosphere)
(b) the albedo is different for different bands. The near infrared band, albedo A_N, is high and the visible-light albedo, A_v is low—this is in accordance with results in Hexi Luzhou; and
(c) the ratio of the visible-light band albedo to the near infrared band albedo (A_v/A_N) equals 0.48.9

In conclusion. for all bands the albedo increases when solar altitude is low and the near infrared albedo is high. This conforms with the results observed in Hexi Luzhou. It should be noted that ground conditions influence the albedo considerably.

Seasonal Variation in Spectral Albedo

The seasonal variation in spectral albedo is shown in Table 3.4, from which the following conclusions are drawn.

Table 3.4: Spectral Distribution of Albedo					
Season	0.2-0.4 μm	0.4-0.5 μm	0.4-0.7 μm	λ > 0.7 μm	0.2-2.8 μm
Spring	0.251	0.0-62	0.182	0.248	0.267
Summer	0.239	0.66	0.122	0.201	0.195
Autumn	2.297	0.049	0.167	0.249	0.270
Winter	0.207	0.052	0.165	0.242	0.245

1) Ultraviolet and near infrared band albedos are high in winter, low in summer, and are the same as the global albedos of all bands. Ground conditions, such as a damp surface with plants in summer, give rise to low ultraviolet and infrared albedos. The snow on the ground makes the albedo greater in winter.

2) The blue-purple band albedo gives opposite results to those described in the previous passage: low in winter and high in summer. The reason for this is that the earth's surface is covered by green plants, making the blue-purple band albedo high in summer because it mostly reflects the wavelength l = 0.55 mm,

3) The near-infrared band albedo is highest (about 34%), the ultraviolet band albedo is about 31 per cent, and the blue-purple albedo is lower than the annual average in Hexi region.

Conclusions

1) In solar spectrum energy distribution, visible-light energy is high and near-infrared energy is comparatively low in Wudaoliang region. There is a difference between the plateau and the plains.
2) Ultraviolet radiation is high in summer and low in winter and blue-purple radiation and near-infrared radiation are low in summer and high in winter.
3) Visible-light energy is high at noon and low in the early morning and late afternoon.
4) Daily variation in the global spectral albedos, A_v, A_N and A_k, is the same, but the variation in A_N is twice as large as that of A_v when the ground is covered with snow. The difference between the value of A_N and A_v is not so great and the variation in A_v is more than in A_N.
5) The ultraviolet band and near infrared albedos are the same as the all-band albedo, i.e., low in summer and high in winter. The blue-purple albedo is high in summer and low in winter.

Further Reading

Baij Jianhui and Wang Gengchen, 1993. 'Basic Characteristics of Solar Ultraviolet Radiation in Beijing Region'. In *Solar Energy Journal*, 14 (3): 245-250.

Jiang Hao, 1993. 'The Spectral Characteristics of Total Solar Radiation and Global Surface Albedo in Heife Luzhou Region'. In *Plateau Atmosphere*, 12 (2): 156-161.

Lin Zhenyao and Wu Xiangding, 1981. 'Regional Planning for Climate in Qinghai and Tibetan Plateau'. In *Geography Journal*, 36 (1): 22-32.

Zhou Yanhua, 1984. Studying for Climatology of Ultraviolet Radiation. In *Solar Energy Journal*, 5 (1) 1-11.

3.4
Direct and Global Solar Radiation in the Region of Mt. Qomolangma During the Summer of 1992

Lu Longhua. Zhou Guoxian and Zhang Zhengqiu

Introduction

The solar radiation in the Mt. Qomolangma Region has always drawn the attention of Chinese and Foreign scholars. Since the 50s, mountaineering expeditions to Mt. Qomolangma have been organized, primarily to study the solar radiation. In summer 1992, an expedition to the Mt. Qomolangma Region took place. Observation sites were established in the Rongbu Temple area (28° 13'N. 86° 49'E. Altitude 4. 950m) and near Mt. Qomolangma. The environmental conditions are similar to those described by Yonguan et al. (1985). From June 30 to August 16, 1992, every fraction of radiation balance was observed by multi-channel remote wire-sensor radiation and the fraction of radiation sequentially observed for 24 hours. The characteristics of direct and global solar radiation in the Mt. Qomolangma Region are presented in the following passages.

Direct Solar radiation

Direct solar radiation was measured by home-made DFY-3 direct radiation meter with a measurement wave band of 0.3-4 mm. The solar radiation outside the atmosphere is 97.85 per cent of the solar constant (1337.6 W/m^2). On August 8, 1992, sunrise took place on Mt. Qomolangma at 7.32 hr (real sun time) local time and the sun set was at 17.02hr. The actual sunrise and sunset were two hours and 12 minutes and one hour and 37 minutes later than astronomical sunrise and sunset,

Figure 3.16 shows the average daily change in direct solar radiation and global solar radiation. When the sky is clear, direct solar radiation in the Mt. Qomolangma region

is 890 W/m^2 shortly after sunrise, about 1. 050 W/m^2 around noon, and 839 W/m^2 before sunset. The daily average value is 976.2 W/m^2. The variation in values measured in a day is under 10 per cent (quadratic mean deviation: 73.9 W/m^2). Furthermore, estimation of direct solar radiation is made by means of global solar radiation (0.2-4 mm) and scattering radiation data obtained from the expedition. If relative deviation and quadratic mean deviation of the measured value (Si) and estimated value (S'i) are given. the values of (a) and (b) can be calculated as follow.

$$a = \frac{\frac{1}{N}\sum S_i \quad \frac{1}{N}\sum S'_i}{\frac{1}{N}\sum S_i} \tag{3.19}$$

$$b = \sqrt{\frac{\frac{1}{N}\sum (S_i - S'_i)^2}{\frac{1}{N}\sum S_i}} \tag{3.20}$$

where N is the number of observations.

When it is clear, the relative deviation of measured value and estimated value at different times (0.3-4.0 mm) is only 1.5 per cent, and the relative quadratic mean deviation is 5 per cent. This shows that the results of the observation are reliable.

Table 3.5 provides the atmospheric transparency during the expedition. The correction of average distance from the sun to the earth and the effect of wave band on the equipment's measurement of solar radiation outside the atmosphere was considered in the course of estimation.

$$P_m = m \sqrt{\frac{S.r}{S_o}} \tag{3.21}$$

P_m Atmospheric transparency coefficient
S Direct solar radiation of vertical ray surface when it is clear
r Correction coefficient of average distance from the sun to the earth, r is 1.03
S_o Solar constant (1367 Wm^{-2}), the wave band of S is 0.3-4.0 mm. solar radiation in the wave band arrived atmosphere outside is 97.85% of the solar constant, thus S is 1337.6 W/m^2.
m Atmospheric optic quality

Table 3.5 also shows that the average atmospheric transparency coefficient in the Mt. Qomolangma region is 0.687. Although the transparency at noon is lower than in the morning and the evening, the relative deviation in the atmospheric transparency coefficient in a day is only 2.4 per cent (quadratic mean deviation: 0.0165).

Table 3.5: Atmospheric Transparency Coefficient in the Mt. Qomolangma Region

Local time	7:41	8:41	9:41	10:41	11:41	12:41	13:41	14:41	15:41	16:41	Ave-rage	QMD
S	890.3	947.1	1010.0	1035.0	1046.0	1054.0	1015	1011.5	914.0	839.0	876.2	73.9
m	1.099	0.800	0.675	0.586	0.560	0.565	0.607	0.700	0.887	1.305		
Pm	0.709	0.674	0.682	0.679	0.680	0.691	0.666	0.700	0.673	0.716	0.687	0.0165

Based on data provided in Yonguan et al.1985, the same methodology was adopted to calculate the atmospheric transparency coefficient in the Rongbu Temple region in the 50s. The result showed that, when it is clear, the atmospheric transparency coefficients at 12:30hr in the region were 0.668 and 0.7116 in June and August 1992 respectively. The result measured by this expedition is close to 0.691. This shows that there is no distinct difference between the state of atmospheric transparency in 1992 and 1959.

Global Solar radiation

All-wave global solar radiation (0.2-4 mm), ultraviolet global radiation (0.295- 0.385 mm), and infrared global radiation (0.7-4.0 mm) were observed by the expedition. Model PSP, Model TUVR, and Model PIRP, products of EPLAB, USA, were used. Daily changes in all-wave band global radiation, ultraviolet global radiation, and infrared global radiation are shown in Table 3.6. From Figure 3.15, it can seen that daily changes from of Q. IR, and UR are coincident on the whole. From Table 3.6, it is observed that ultraviolet radiation accounts for 3.74 per cent of global radiation and infrared global radiation accounts for 63.2 per cent of global radiation. The percentage changes of ultraviolet and infrared are small in one day (the quadratic mean deviations are 0.07 and 1.15 per cent respectively and account for 1.9 per cent of the average value). The maximum value of ultraviolet radiation was 62 W/m², corresponding to the maximum value of ultraviolet radiation in the west pacific equatorial region.

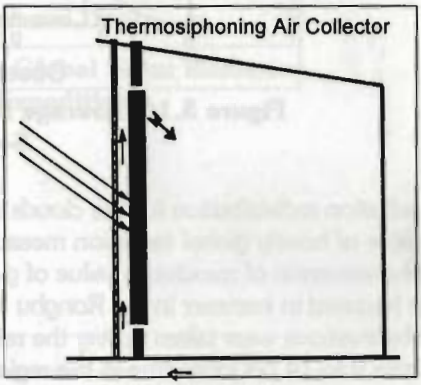

Figure 3.15:

It is not unusual for the maximum value of global radiation to be greater than the solar constant in the Qinghai-Xizang Plateau area. This phenomenon is the result of solar

Table 3.6: Global Radiation. Ultraviolet Radiation and Infrared Radiation in the Mt Qomolangma Region

Local time	7:41	8:41	9:41	10:41	11:41	12:41	13:41	14:41	15:41	16:41	Average	AMD
Q	517.0	776.5	1002.8	11.97	1439.3	1458.0	12162	975.0	729.4	424.0	823.0	489.0
UR	19.3	29.1	38.0	44.8	53.0	53.0	48.0	37.3	26.7	16.0	33.6	16.1
IR	324.0	490.7	636.8	754.8	893.7	899.0	808.7	627	452.2	277.0	520	302.8
UV/ Q(%	3.7	3.8	3.8	3.7	3.7	3.6	3.8	3.8	3.7	3.8	3.7	0.07
IR /Q (%)	62.7	63.2	63.5	63.0	62.1	61.7	64.1	64.4	62.0	65.3	63.2	1.15

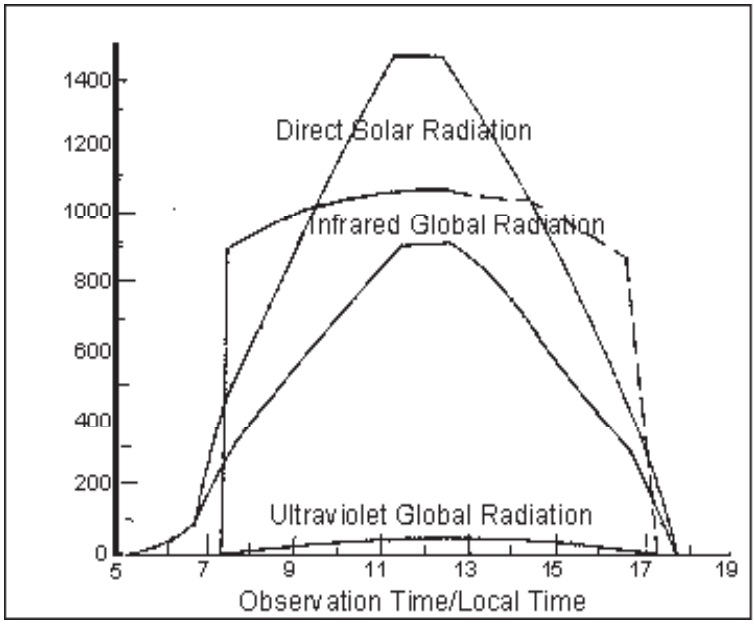

Figure 3.16: Average Daily Change in Direct and Global Solar Radiation

of solar radiation redistribution for the clouds in alpine areas. Figure 3.16 gives the maximum value of hourly global radiation measured. From the figure, we can see that the phenomenon of maximum value of global radiation being greater than solar constant is frequent in summer in the Rongbu Temple region of Mt. Qomolangama. The observations were taken during the rainy season. The phenomenon could be observed from 9 to 14 hrs local time in the region of Rongbu Temple. Mt. Qomolangma; it sometimes occurred as much as five times sequentially. The maximum value of instantaneous global radiation was 1688 W/m^2 (15:07, 5, August), which is 23 per cent greater than the solar constant. During the expedition, the maximum value of hourly amounts of global radiation recorded reached 4.71 MJ/m^2 (10:41-11:41, 4, August); the average intensity was 1308 W/m^2, i.e., 95.7 per cent of the solar constant.

Figure 3.17 gives the maximum value of instantaneous global radiation at different altitudes. Above 500m, the relationship between the maximum value of instantaneous global solar radiation and altitude can be expressed by:

$$Qmax = 157.346 \log_e(Z) + 274.548 \qquad (3.22)$$

On the northern summit of Mt. Qomolangma, the value of instantaneous global radiation measured was 1382 W/m^2. According to Equation 3.5.4, the maximum value of global radiation in the region is 1700 W/m^2. It can be observed that instantaneous global solar radiation is greater than solar constant at low altitudes. These sites are usually islands, and the radiation reflected from the clouds can be substantial. In low altitude areas, the reflection of the clouds plays an important role in the occurrence of this phenomenon—which is only for a short duration. In the Alpine region on the

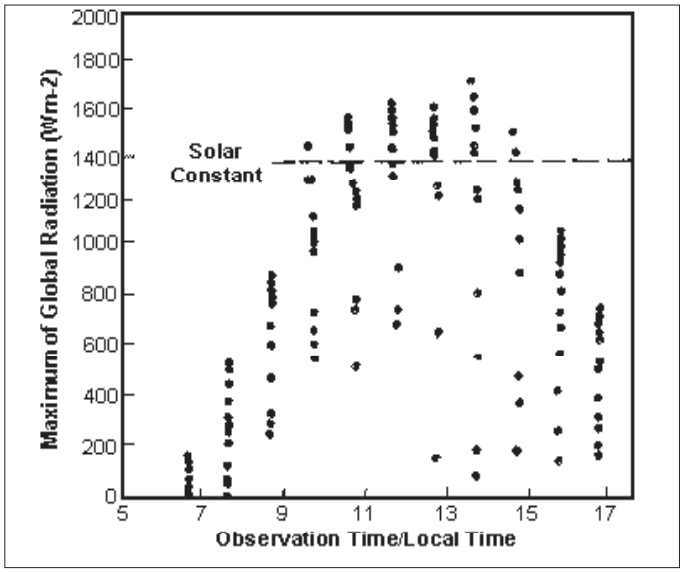

Figure 3.17: Maximum Hourly Global Solar Radiation Recorded by the Expedition

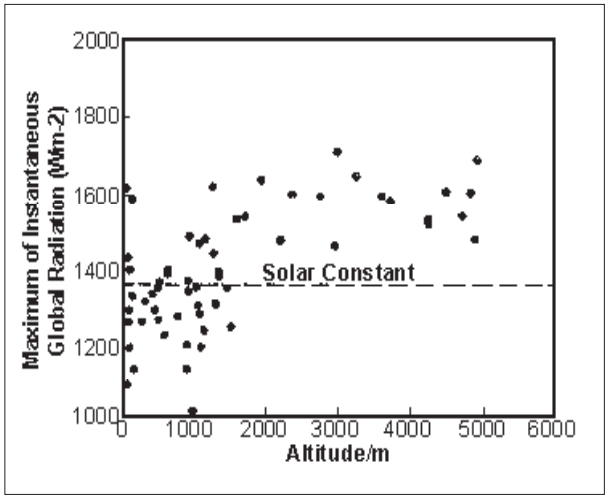

Figure 3.18: Relationship between the Maximum Value of Instantaneous Global Radiation and Altitude

other hand, one can have very strong direct radiation quite often. The phenomenon of instantaneous solar global radiation being greater than the solar constant in the plateau region of Quinghai-Xizang needs further study.

Further Reading

Kou Youguan; Zeng Qunzhu; and Yie Weirong, 1985. *Solar Radiation in the Region of Mt. Qomolangma. Report of Science Expedition to the Region of Mt. Qomolangma (1966-1968)*. Beijing: Science Press.

Lu Longhua and Dai Jiaxi, 1997. 'Global Solar Radiation and Net Radiation in Tanggula Region'. In *Science Bulletin*, 1979.9 (24): 400-404.

Yao Lanchang; Yuan Fumao; and Cheng Youyau, 1986. 'The State of Solar Radiation in the West Pacific Equatorial Sea Area in Autumn. 1986 and 1987'. In *Plateau Meteorology*. 1989.8 (4): 331-344.

Zhou Xiuji; Tao Shanchang; and Yao Keya, 1991. *High Atmospheric Physics*. Beijing: Meteorology Press.